JOURNAL OF MATERIALS SCIENCE 24 (1989) 133–138

TEM study of the microstructure of carbon–carbon composite

W. KOWBEL
Materials Engineering, Department of Mechanical Engineering, Auburn University, Auburn, Alabama 36849, USA

J. DON
Department of Mechanical Engineering and Energy Processes, Southern Illinois University, Carbondale, Illinois 62901, USA

A detailed study of the structure of carbon–carbon composite was performed using transmission electron microscopy (TEM) techniques. Structural characterization is essential in order to understand fully the mechanical and physical properties of these materials. The use of an atom mill in sample preparation made it possible to perform TEM analysis on the fibres, matrix, and the fibre–matrix interface. Full characterization of the fibres was performed across the fibre diameter. Structural heterogeneity was characterized in terms of preferred orientation Z, stack height L_c, stack width L_a, and d_{002} spacing. The use of 0 0 2 dark field imaging showed the orientation and size of turbostratic and graphitic crystallites in the fibre and the matrix. Amorphous resin was located in the interbundle matrix.

1. Introduction

Transmission electron microscopy (TEM) has been extensively used to study carbon materials [1, 2]. This technique offers a way of characterizing the microstructure in several modes. Electron diffraction techniques (SAD, microdiffraction) have permitted the structural characterization of carbon materials in terms of four parameters, Z, L_c, L_a, and d_{002} [3, 4]. Electron diffraction has been useful in cases in which the longitudinal or transverse structure possesses structural heterogeneity. Using the smallest aperture (SA) it is possible to select any region, as small as 0.8 μm, and obtain its selected area diffraction pattern. This pattern can be analysed by using a scanning densitometer; the diffraction peaks can be analysed by analogous methods, as used in X-ray diffraction [1]. Bennet [5] showed, by using electron diffraction, that some Type I carbon fibres can have skin–core heterogeneity. The skin was more oriented and had larger crystallites than the core, but was never more than 250 nm thick.

Application of scanning transmission electron microscopy permits microdiffraction in both TEM and STEM modes from an area as small as 4 nm, providing an excellent technique for the study of microcrystallinity.

Dark field micrographs using 0 0 2 reflections of the diffraction pattern have been used to estimate the crystallite size [6] and to show that the surface crystallites are larger in size than the core crystallites [5]. The importance of dark field imaging has been emphasized by Oberlin [7]. She has suggested that the differentiation between the fibrillar and the lamellar models of carbon fibres can be made only through very careful comparison of (1 1) and (1 0) dark field images. By the use of dark field high resolution micrographs for pitch and PAN based carbon fibres, Oberlin has demonstrated that the lamellar model best describes the microstructure of the fibres. The application of 0 0 2 lattice resolution has led to two existing models of carbon fibres by Johnson [1] and Oberlin [7]. Johnson's model suggests interpenetration of the carbon layers in addition to the intermingling of the layers. Oberlin's model consists of large sheets of carbon layer stacks crumpled, distorted, and intermingled with an apparent skin and core effect. In the second model, crystallites at the fibres' surface are partially graphitic at most, with only a few pairs of carbon layers possessing graphitic order.

The increasing market for carbon–carbon composites in aerospace applications has sparked an extensive research interest in these materials. Their structure has been characterized by optical microscopy, SEM and SAD [8, 9]. Results showed major differences in crystallographic orientations and graphitic order within the individual structural components. Carbon fibres have shown skin–core heterogeneity. The interbundle and intrabundle matrices are highly graphitic and show high orientation parallel to the fibre axis at interfacial regions. The knowledge of the microstructure of the composite can be related to the mechanical and oxidation properties. The degree of preferred orientation in the fibres and the matrix can be related to the elastic properties of the composite, that is, the more highly oriented the layer planes, the higher the tensile modulus [10].

In terms of oxidation for a given carbon material,

0022–2461/89 $03.00 + .12

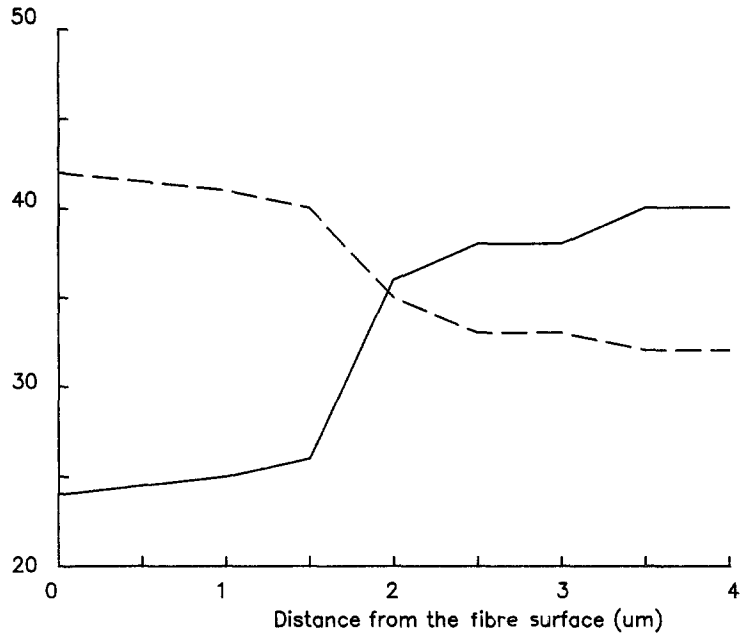

Figure 1 The changes in microstructure across a fibre. (—— Z (deg), – – – L_c (nm)).

the rate of oxidation decreases with increased degree of graphitization [8].

Preparation of a thin sample of structural carbon for electron microscopy is a complex task. In the case of carbon fibres, ultramicrotomy has recently been used by several researchers. This technique results in a highly shredded thin film of carbon fibres.

Presented in this manuscript will be the application of the atom milling technique to obtain thin specimens of longitudinal and transverse sections of three-dimensional carbon–carbon composites. Thin sections of the fibres, matrices and the interface are analysed by electron diffraction techniques, bright field and dark field images. The structural heterogeneity of carbon–carbon composite is discussed in detail.

2. Materials used

An industrially supplied three-dimensional carbon–carbon composite consisting of polyacrylonitrile based carbon fibres impregnated with coal tar pitch matrix was used. The composite was prepared by several high pressure impregnation carbonization process. The process is based on multiple pitch impregnation–carbonization at high pressures and graphitization cycles to densify the composite.

3. Transmission electron microscopy

For TEM analysis, specimens of about 500 μm thick were cut from the block of composite using a diamond saw. Three millimetre discs were cut from each slice using a drilling machine. The discs were further dimpled in a four-stage process to obtain about 10 μm thick specimen at the centre. The discs were milled by using an Ion Tech atom mill at the initial incidence angle of 45°. The total ion current of 2 mA and voltage of 5 kV was employed. Following specimen perforation, the milling angle was lowered to 12°. The final specimen had several very thin areas suitable for TEM observations.

The TEM observations were performed with a Hitachi 500 electron microscope operating at 100 kV. Bright field images were taken at 5000 to 100 000 magnification by using the smallest objective aperture (20 μm). The 0 0 2 and 1 0 0 dark field images were obtained by tilting the incident beam so the 0 0 2 and 1 0 0 spots, respectively, coincided with the optical axis of the microscope. The smallest objective aperture was then used to remove all other reflections. SAD patterns were obtained by using the smallest aperture.

Equatorial or meridional traces of diffraction patterns were obtained by using scanning densitometers. The peaks resolution was performed by assuming Gaussian shape of the peaks and subtracting the background. Assumed Gaussian peak shape was found to introduce a negligible error. The parameters of the resolved peaks were then used to find half width or integral breadth. The crystallite size was found by the Scherrer equation, $L = k/\Delta S$. L_a was determined from the 1 0 0 medidional reflection, with $K = 1$. When the order of 0 0 L reflection was 0 0 2, L_c was evaluated, with $K = 1.0$. With two or more resolutions, the expression $\Delta S = K/D_c + 2\pi^2\sigma^2L^2$ [5], where D_c is mean free distance, σ is the r.m.s. local distortion ($\Delta d/d$) in the layer spacing d, and K taken as 1 was used. The preferred orientation Z was measured as the full width at half maximum peak intensity of an azimuthal microdensitometer scan of 0 0 2 reflection, and d_{002} was calculated from the position of the 0 0 2 peak.

The microdiffraction patterns were obtained on a Philips 420 TEM microscope equipped with STEM attachment operating at 120 kV. Both nano and microsize diffraction in TEM mode were obtained. The smallest probe was of about 4 nm.

4. Results

Transmission electron microscopy was carried out on both longitudinal and transverse sections of the carbon–carbon composite. Fig. 2 shows the transmission electron microscope micrograph of the matrix (positon B) and the fibres (position A) in the longitudinal section. The intrabundle matrix has a width less than 1 μm, suggesting volume fraction of fibres

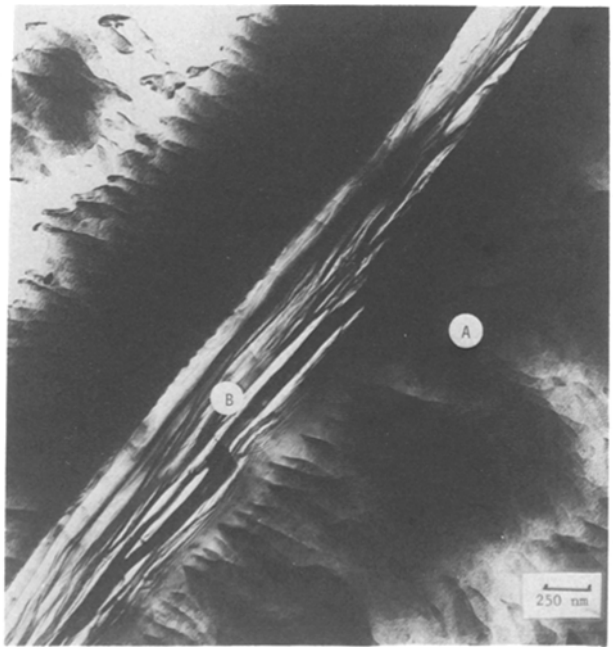

Figure 2 TEM micrograph of the longitudinal section of the carbon–carbon composite.

more thasn 75%. The intrabundle matrix is composed of several sheet-like structures running parallel to the fibre axis. Microcracks can be observed between the graphitic plates. Carbon fibre shows the rippling structure, which is the result of the milling technique used in sample preparation, as reported by Goodhew [11]. Fig. 3 shows the transmission electron microscope micrograph of the transverse section of carbon–carbon composites. Carbon fibre shows two distinctive structures which are separated by the annulus, the outer sheath ($\sim 2\,\mu$m wide) (position B) and the core ($4\,\mu$m wide) (position C). The annulus has an appearance of the interphase between the outer part and the core. The difference in orientation between region B and region C could possibly result in the generation of the residual stresses at the interphase upon manufacturing. The build-up of these stresses can lead to possibly non-uniform thickness distribution upon sample preparation. Thus the dark area can represent larger thickness due to structural heterogeneity and the subsequent residual stresses generation.

The intrabundle matrix (position A) is well aligned around the fibre surface, and π and 2π disclinations in the intrabundle matrix can be observed between an assembly of three or four fibres. This observation is consistent with the work of Zimmer [12], who

TABLE I The changes in the structural parameters across the fibre diameter

Distance from the fibre surface (μm)	Z (deg)	L_c (nm)	L_a (nm)	d_{002} (nm)
0	24	4.2	6.5	0.342
1.0	25	4.1	6.3	0.342
1.5	26	4.0	6.3	0.342
2.0	36	3.5	6.3	0.344
2.5	38	3.3	6.2	0.344
3.0	38	3.3	6.2	0.344
3.5	40	3.2	6.2	0.344
4.0	40	3.2	6.2	0.344

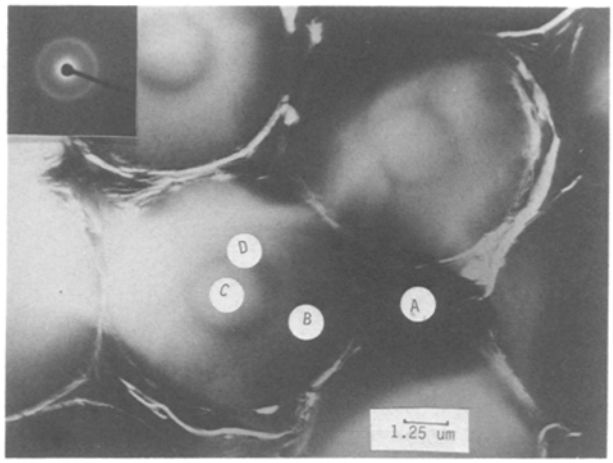

Figure 3 TEM micrograph of the transverse section of the carbon–carbon composite.

confirmed the presence of the disclinations with $S = -\frac{1}{2}$ in the triangular array of the fibres and the disclinations $S = -1$ in the square array of the fibres by polarized optical microscopy. The resemblance of the white areas arrangement in Fig. 3 to that described by Zimmer is the basis for the statement, that disclinations can be present in the intrabundle matrix. In longitudinal section, the SAD patterns were taken across the fibre diameter, which revealed structural heterogeneity in terms of only two zones, a better oriented outer zone, $Z = 22°$, and a more misoriented core, $Z = 40°$. The crystallite stack height is larger in the outer zone, $L_c = 4.2$ nm, compared to 3.2 nm in the core (Table I). Since the error in L_c calculations is only 0.2 nm, the difference between the core and the outer part is clear. Thus, SAD results did not confirm the annulus as observed in the transverse section to be a structurally distinctive region. These data are plotted in Fig. 1. The outer sheath is about $2\,\mu$m and consists of much more organized, slightly larger crystallites. The core is about $4\,\mu$m thick and consists of less oriented, smaller crystallites. The SAD patterns typical for the outer sheath and the inner core are shown in Fig. 4c, insets. The 0 0 2 arc for the outer part are much smaller, indicating clearly higher orientation of crystallites in the outer part. Lack of (1 1 2) ring in both patterns indicates that the carbon fibre is turbostratic. The crystallite size, as detected by SAD, differs only in terms of L_c. The crystallite stack width, L_a, does not differ and is about 6.3 nm. The 0 0 2 dark field images of the longitudinal section of the fibre are shown in Fig. 4. Figs 4a and b show the outer part and the core of the fibre, respectively. Fig. 4c shows the interfacial region between the two structural zones. Position A, Fig. 4c, represents the outer part of the fibre, while position B, Fig. 4c, represents the core. The white areas represent the crystallites. It can be observed that the crystallites in the outer part are larger and more oriented, as shown by the 0 0 2 dark field. The annulus, as observed in bright field, is not confirmed by the dark field observation. Thus, the two zone structure of the fibre, as observed in the SAD observation, is confirmed by the 0 0 2 dark field images. The SAD patterns taken in transverse section, Fig. 3, all showed 0 0 2 ring instead of 0 0 2 arc, which was

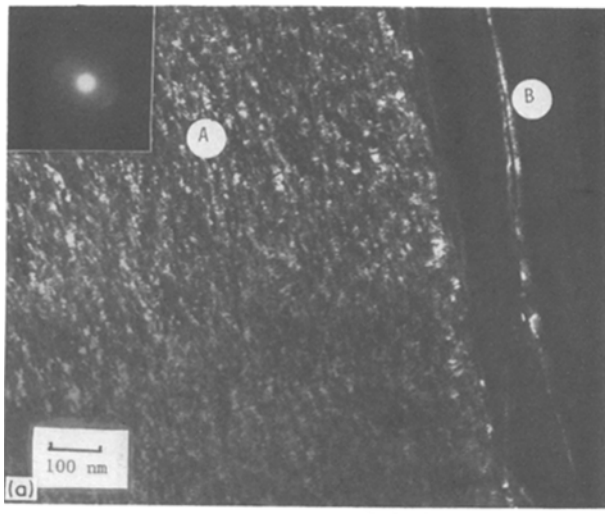

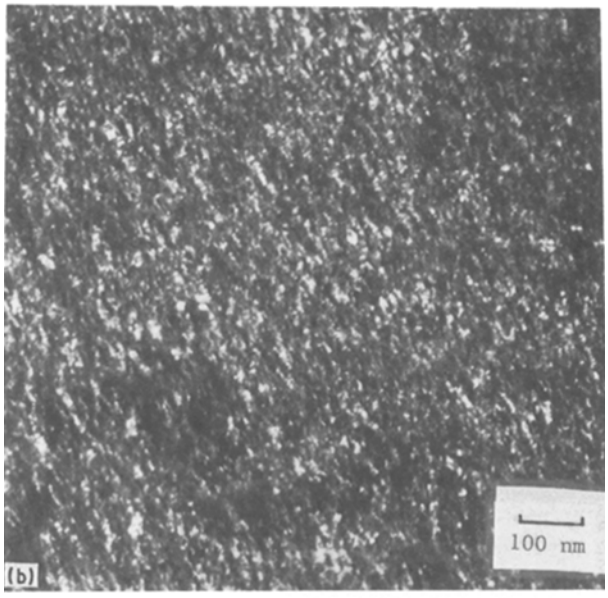

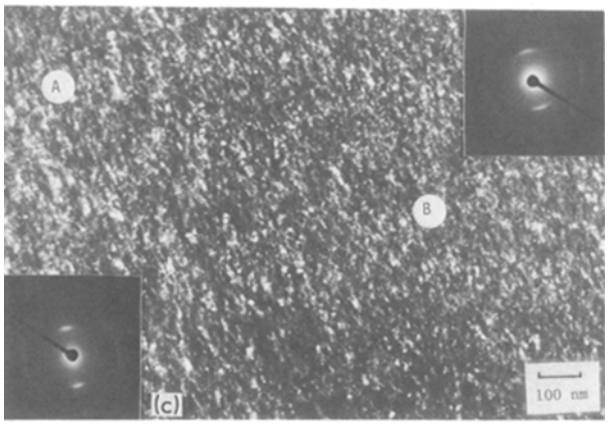

Figure 4 (a) The 0 0 2 dark field of the outer part of the fibre. (b) The 0 0 2 dark field of the core of the fibre. (c) The 0 0 2 dark field of the fibre showing the interface between two structural zones.

TABLE II The structural parameters for the matrix in carbon–carbon composite

Region	Z (deg)	L_c (nm)	L_a (nm)	d_{002} (nm)
Intrabundle matrix	18	12.0	21.0	0.336

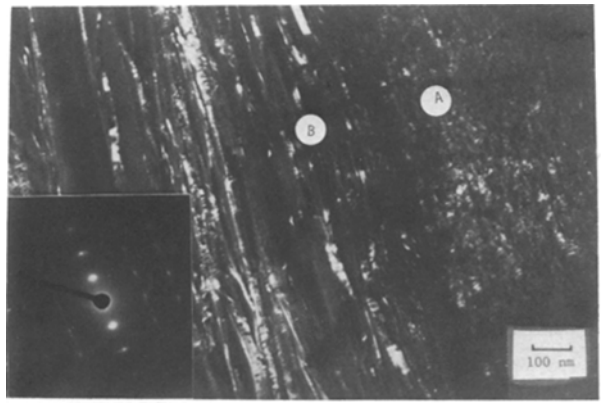

Figure 5 0 0 2 dark field of the intrabundle matrix.

observed in longitudinal section. This suggests a random orientation of basal planes in the transverse section. The SAD pattern for the intrabundle matrix is shown in Fig. 5, inset. The intrabundle matrix is graphitic, with well defined *hkl* reflections. The structural parameters, Table II, showed $Z = 18°$, $L_c = 12.0\,nm$, $L_a = 21.0\,nm$, $d_{002} = 0.336\,nm$. The error in d_{002} calculation is about 0.006 nm. Thus, the differences in d_{002} cannot be used as a confirmation of the graphitic structure. The difference can be shown by the presence or absence of $h\,k\,l$ reflections.

These results indicate that the intrabundle matrix is highly graphitic, $d_{002} = 0.336\,nm$. The preferred orientation, $Z = 18°$, suggests that the orientation of the graphitic crystallites in the intrabundle matrix is higher than in the outer part of the fibre. The values of L_c and L_a for the intrabundle matrix are much larger than the corresponding crystallite sizes for the turbostratic crystallites in the fibre.

The 0 0 2 dark field of the intrabundle matrix is shown in Fig. 5. The graphitic crystallites in the intrabundle matrix (position B) are bigger and more oriented than the turbostratic crystallites of the outer part of the fibre (position A). They exhibit high orientation in the direction of the fibre axis, which confirms SAD results.

Fig. 6a shows the bright field of the interbundle matrix, showing large graphitic crystallites represented by dark areas. Those crystallites do not exhibit high preferred orientation as the crystallites in the intrabundle matrix.

Fig. 6b shows the 0 0 2 dark field of the interbundle matrix. Again, large graphite crystallites can be seen. The typical SAD pattern of the interbundle matrix is shown in Fig. 6b, inset. The SAD pattern clearly shows the presence of three-dimensional graphite in the interbundle matrix, indicated by the presence of (1 1 2) ring. The 0 0 2 arc is composed of several 0 0 2 spots, each of which represents a different graphite crystal.

The microdiffraction pattern of the fibre, Fig. 4a, inset, shows large 0 0 2 arc, indicating that the turbostratic structure has a significant amount of misorientation, parameter $Z = 35°$. Since the microdiffraction pattern was obtained from the area as small as 4.0 nm, the carbon stacks within one crystallite have to be non-planar.

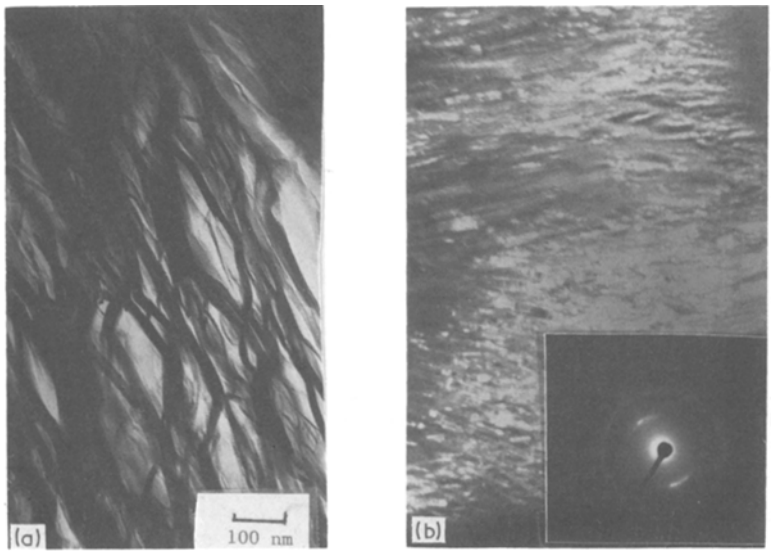

Figure 6 (a) Bright field of the interbundle matrix. (b) 0 0 2 dark field of the interbundle matrix.

5. Discussion

Transmission electron microscopy offers a comprehensive way of analysing the microstructure of composite material, like carbon–carbon composites. The use of the atom milling technique allows study of large areas of carbon–carbon composites, including the fibres, the matrix, and the interphase. The carbon–carbon composite analysed in this work is composed of turbostratic fibres and graphitic matrix. The fibres showed structural heterogeneity in terms of degree of preferred orientation and the crystallite stack height, L_c. The outer part of the fibres has a higher degree of preferred orientation, $Z = 24°$, compared to the less oriented core, $Z = 40°$. The more oriented outer sheath has a width of about 1.5 μm. The structural heterogeneity can also be observed in the transverse section bright field picture, Fig. 3. These two structures are separated by a ring, which is clearly shown in Fig. 3. This ring possibly represents the interphase between two areas of different degree of the orientation and as a result of the thermal stresses introduced in the processing this interphase can possibly be under a residual stress.

Although the work by Bennet and Johnson [5] showed that some Type I fibres can have a skin–core heterogeneity, the fibres studied in this work showed significant structural changes to those studied by Bennet. The outer sheath reported here is about 1.5 μm, compared to, at the most, 0.5 μm thick sheath observed by Bennet. In both cases, crystallite stack height, L_c, was increasing toward the skin; however, the size differences between the crystallites in the outer part and the core is much smaller compared to that found by Bennet.

In both cases, the orientation of the outer sheath is higher than the orientation of the core. Since all fibres studied by Johnson and Bennet were graphitized in a free state, the mode of graphitization might influence the formation of wider outer zone, as observed in this study. Thus, the stress graphitization with applied mechanical forces can ultimately alter the resulting structure of the fibres, since the fibres in the composite were graphitized in the presence of the pitch matrix. The variation of the structure as a function of the distance from the centre of the fibre is crucial to understanding the variation of Young's modulus and resulting residual stresses.

The structural heterogeneity across fibre diameter in terms of changes in preferred orientation, will result in the gradation of Young's modulus across fibre diameters. Since the Young's modulus increases strongly with higher preferred orientation, the outer part of the fibre should have a higher Young's modulus. This is in good agreement with Diefendorf's experiments [13]. The gradation in microstructure existing in the fibres should result in residual stresses upon cooldown process, leaving the outer part in compression and the core in tension. The effect of surface compression may minimize the effect of surface flaws, increasing the tensile strength of the fibres. The crystallite size, L_c, also varies across the fibre diameter. The crystallites are larger on the surface compared to the bulk. Assuming the Reynolds–Sharp mechanism of failure for Type I carbon fibres, larger crystallites on the surface may be a strength limiting factor, lowering tensile strength of graphitized fibres compared to only carbonized carbon fibres.

The SAD pattern of the fibre transverse section shows the 0 0 2 ring, indicating no preferred orientation in the transverse section. The SAD studies of the intrabundle matrix showed a high degree of preferred orientation, Table II, higher even than the outer part of the fibre. The structure is graphitic, with a higher crystallite size than turbostratic crystallites in the fibre. The high degree of preferred orientation in the intrabundle matrix may be explained by the mesophase transformation. The carbon–carbon composite studied in this work was obtained by fibres infiltration with the pitch. During the heat treatment, the pitch underwent mesophase crystallization. Apparently, the presence of the fibres acted as a substrate and resulted in the orientation of mesophase crystallites in the direction of the fibre axis. This orientation was further improved in the subsequent carbonization and graphitization processes, resulting in large graphitic crystallites predominantly aligned along the fibre axis. The high orientation of the

graphite crystallites in the intrabundle matrix should significantly improve the longitudinal Young's modulus of the bundle. Some of these crystallites are misoriented with respect to the fibre axis, Fig. 5. Since the Young's modulus increases with the improved preferred orientation, the mesophase transformation is crucial to the development of highly orientated intrabundle matrix. If the carbon–carbon composite is made by pyrolysing the resin, the Young's modulus should be much lower compared to the carbon–carbon composite obtained by pitch infiltration. This is a direct result of the fact that the resin will form glassy carbon after pyrolysis and will not exhibit preferred orientation. Since the crystallite size in the intrabundle matrix is larger than in the fibres, in the oxidation behaviour, the matrix will be expected to oxidize at a slower rate, assuming the same level of impurities. The studies of the interbundle matrix reveal large graphitic crystallites, which can exhibit some orientation on submicrometre scale, Fig. 6b. Since the interbundle matrix has the largest crystallite size in the carbon–carbon composite, its oxidation resistance is expected to be the best, again assuming the same level of impurities. However, the presence of impurities in the matrix can catalyse the oxidation and lower the resistance against oxidation. The bright field of the transverse section of the composite shows that the intrabundle matrix is aligned around the fibres and has many disclinations. The presence of these disclinations will be another factor limiting significantly the strength of the carbon–carbon composites.

6. Conclusions

Carbon–carbon composite has a very complex structure, as revealed by TEM study. The carbon fibres exhibit structural heterogeneity in terms of core–sheath structure. This will result in higher modulus of the outer part of the fiber and residual stresses resulting from thermal processes. As a result, the outer part of the fibre will be under compression. The crystallite size distribution in the fibre is also non-uniform. The larger crystallite size in the outer part causes the fracture to be surface limited. The intrabundle matrix is graphitic, highly oriented, leading to better stiffness properties of the whole composite. The structural heterogeneity of the composite will affect both the mechanical and oxidation properties. Since the matrices are more graphitic than the fibres, their oxidation resistance should be greater.

Acknowledgement

This work was supported by the Materials Technology Center, Southern Illinois University.

References

1. D. J. JOHNSON and D. CRAWFORD, *J. Mater. Sci.* **8** (1973) 286.
2. A. OBERLIN, *Scanning Electron Microsc.* (4) (1982) 1523.
3. B. J. WICKS, *J. Mater. Sci.* **16** (1971) 173.
4. A. OBERLIN, *ibid.* **23** (1982) 7.
5. S. C. BENNET and D. J. JOHNSON, *ibid.* **14** (1976) 117.
6. D. V. BADAMI, J. C. JOINER and G. A. JONES, *Nature* **215** (1967) 386.
7. A. OBERLIN, *Carbon* **17** (1979) 7.
8. L. E. JONES and P. A. THROWER, *Carbon* **26** (1986) 51.
9. W. MURDIE, E. J. HIPPO and W. KOWBEL, *Carbon*, submitted.
10. W. RULAND, *Appl. Polym. Symposia*, No. 9. (1969) 293.
11. P. J. GOODHEW, in "Practical Methods in Electron Microscopy", Vol. 1, edited by A. M. Glauert, p. 161.
12. J. E. ZIMMER, *Carbon* **21** (1983) 328.
13. F. J. DIEFENDORF, in "Progress in Science and Engineering of Composites", Vol. 1, edited by T. Hayashi (New York, 1983) p. 85.

Received 17 August 1987
and accepted 2 June 1988